Published in final edited form as:
Atherosclerosis. 2012 January ; 220(1): 78–85. doi:10.1016/j.atherosclerosis.2011.10.020.

Relationship between hemodynamics and atherosclerosis in aortic arches of apolipoprotein E-null mice on 129S6/SvEvTac and C57BL/6J genetic backgrounds

Hirofumi Tomita,
Department of Pathology and Laboratory Medicine, The University of North Carolina at Chapel Hill, Chapel Hill, NC 27599-7525, USA

John Hagaman,
Department of Pathology and Laboratory Medicine, The University of North Carolina at Chapel Hill, Chapel Hill, NC 27599-7525, USA

Morton H. Friedman[*], and **Nobuyo Maeda**
Department of Pathology and Laboratory Medicine, The University of North Carolina at Chapel Hill, Chapel Hill, NC 27599-7525, USA

[*]Department of Mechanical and Aerospace Engineering, The George Washington University, Washington DC 20052, USA

Abstract

Objective—We investigated the relationships between hemodynamics and differential plaque development at the aortic arch of apolipoprotein E (apoE)-null mice on 129S6/SvEvTac (129) and C57BL/6J (B6) genetic backgrounds.

Methods—Mean flow velocities at the ascending and descending aorta (mVAA and mVDA) were measured by Doppler ultrasound in wild type and apoE-null male mice at 3 and 9 months of age. Following dissection of the aortic arches, anatomical parameters and plaque areas were evaluated.

Results—Arch plaques were five times bigger in 129-apoE than in B6-apoE mice at 3 months, and twice as large at 9 months. The geometric differences, namely larger vessel diameter in the B6 strain and broader inner curvature of the aortic arch in the 129 strain, were exaggerated in 9-month-old apoE-null mice. Cardiac output and heart rate under anesthesia were significantly higher in the B6 strain than in the 129 strain. The values of mVAA were similar in the two strains, while mVDA was lower in the 129 strain. However, there was a 129-apoE-specific reduction of flow velocities with age, and both mVAA and mVDA were significantly lower in 129-apoE than in B6-apoE mice at 9 months. The mean relative wall shear stress (rWSS) over the aortic arch in 129-apoE and B6-apoE mice were not different, but animals with lower mean rWSS had larger arch plaques within each strain.

Correspondence to Nobuyo Maeda, PhD Department of Pathology and Laboratory Medicine, The University of North Carolina at Chapel Hill, CB #7525, 701 Brinkhous-Bullitt Building, Chapel Hill, NC 27599-7525 Tel: +1-919-966-6912 Fax: +1-919-966-8800 nobuyo@med.unc.edu.

Disclosures The authors have no conflicts to disclose.

Conclusions—The plaque formation in the arch of apoE-null mice is accompanied by strain-dependent changes in both arch geometry and hemodynamics. While arch plaque sizes negatively correlate with mean rWSS, additional factors are necessary to account for the strain differences in arch plaque development.

Keywords

Apolipoprotein E-null mouse; Atherosclerosis; Aortic geometry; Hemodynamics; Wall shear stress

Introduction

Hemodynamic factors such as wall shear stress (WSS) influence substantially the distribution of atherosclerotic lesions and play a major role in the regional development of atherosclerotic plaques (1-3). Atherosclerotic lesions in humans develop preferentially along the inner wall of curved segments and at the bifurcations of relatively large arteries, where WSS is significantly lower than in other regions. The pattern and the spatial distribution of atherosclerotic plaques in these areas vary from one individual to another. In addition, large inter-individual variations in vascular anatomy, such as the bifurcation level of the common carotid artery and variations of the coronary artery, have been related to differences in plaque formation in humans (4-7).

Apolipoprotein E (apoE)-null mice spontaneously develop atherosclerotic plaques at the aortic arch and aortic root (8,9). Previously, we found that there are strain-specific differences in the distribution of atheroma in the aorta (9,10). The lesions at the aortic arch in apoE-null mice on a 129S6/SvEvTac background (129-apoE) develop more rapidly compared to those on a C57BL/6J (B6-apoE) background, in spite of a slower development of lesions at the aortic root. Moreover, the shape of the aortic arch clearly differs in the two strains (10,11). Accordingly, this pair of strains of apoE-null mouse allows us to explore the relationships among atherosclerosis, hemodynamics, and vascular geometry.

Doppler ultrasound is a noninvasive and repeatable method of measuring hemodynamic parameters. Hartley et al have reported that there is a difference in the magnitude and shape of the aortic arch velocity signal between 13-month-old apoE-null and wildtype (WT) mice on a B6 genetic background (12). This finding could reflect to some extent the effect of the atherosclerotic lesions themselves on the hemodynamic parameters at the aortic arch. In the present study, we tested the hypothesis that differences in aortic geometry between the two strains affect hemodynamics, and consequently contribute to the differences in plaque development at the aortic arch. We found that the two strains show different patterns of hemodynamics, which are exaggerated by the arch plaques in a strain-dependent manner. Our data further demonstrate a significant interaction between mean relative WSS over the entire aortic arch and plaque extent, indicating a strain-independent role of WSS in arch plaque development.

Methods

Detailed methods are available in the Supplement. WT and apoE-null male mice on 129S6/SvEvTac and C57BL/6J backgrounds at 3 and 9 months of age were used. Heart function and blood flow velocity were measured at the ascending and descending aorta using a Vevo770 imaging system (VisualSonics, Toronto, ON, Canada) as previously described (13,14). A large pulsed Doppler sample volume was placed to cover the entire aortic lumen at stations in the ascending and descending aorta (L1 and L2, respectively, Figure 1B). Mean flow velocities at the ascending aorta (mVAA) and descending aorta (mVDA), averaged

over systole, were quantified. To evaluate local flow distribution across the aortic lumen, a small Doppler sample volume (axial dimension 220 or 270 μm, Vevo2100 imaging system, VisualSonics) was placed at the region close to the outer curvature and the region close to the inner curvature in the ascending aorta (L1) and descending aorta (L2). Systolic mean velocity along both curvatures and the early diastolic time-velocity integral (TVI) along the inner curvature were measured.

Anatomical parameters and plaque areas at the aortic arch and root were measured as previously described (10). Briefly, after perfusion of mice with 4% paraformaldehyde under physiological pressures, the aortic tree was dissected free of surrounding tissue under a dissection microscope and its images were captured (Figure 1A and 1F). The diameters of the ascending aorta (AA) and descending aorta (DA), inner curvature of the aortic arch (angle, Figure 1B), and plaque lesion sizes in the inner curvature of the aortic arch were measured using Image J 1.40.

All data are expressed as mean±SEM. The significance of the effects (age, strain, and genotype) and their interactions were determined by three-way ANOVA (Supplemental Table).

Results

Characteristics of the mice

Physiological profiles of the male mice we studied show that the mice on a B6 background weighed more than those on a 129 background in all groups (Table 1). Total cholesterol levels were higher in the 129 strain than in the B6 strain, particularly in apoE-null mice. HDL-C levels were also significantly higher in the 129 strain than in the B6 strain in both WT and apoE-null mice at 9 months of age. Hematocrit was significantly higher in the 129 strain than in the B6 strain regardless of apoE genotype and age. In contrast, platelet count was significantly higher in the B6 strain in all groups. At 9 months, B6-apoE mice exhibited a significantly higher fractional shortening than 129-apoE mice. Significant age effects were found in heart weight and in stroke volume, but no strain effects were observed. Heart rate under anesthesia was significantly higher in the B6 strain than in the 129 strain across the four groups. Similarly, cardiac output in the B6 strain was significantly higher than that in the 129 strain in 3-month-old WT and 9-month-old apoE-null mice. However, systolic blood pressure and pulse rate measured by the tail-cuff method in conscious mice at 9 months of age were not significantly different (Supplemental Figure 1).

Anatomical differences between the two strains

The diameter of the ascending aorta (AA) measured using captured images positively correlated with the end-systolic diameter of the ascending aorta evaluated by echocardiography (R^2=0.34, $p<0.01$, n=20), but not as strongly with the end-diastolic diameter (R^2=0.17, p=0.07, n=20). This indicates that the AA diameter measured in the captured image is a reasonable representation of the diameter of the ascending aorta at end systole, and we used this value in the following analyses. The AA diameter was significantly larger in the B6 strain than in the 129 strain in both WT and apoE-null mice (Figure 1C). There was also a significant strain effect ($p<0.05$) on the diameter of the descending aorta (DA), particularly in apoE-null mice at 9 months (Figure 1D). Of note, both the AA and DA of B6-apoE mice at 9 months were significantly larger than those of B6-WT mice at 9 months, but this difference between genotypes was not seen in the 129-apoE mice. The angle BAC was wider in the 129 strain compared with the B6 strain in both WT and apoE-null mice (Figure 1E). Moreover, while age and genotype did not affect the angle in the B6 strain, 129-apoE mice at 9 months had a wider angle than 129-WT mice at 9 months. Thus,

vascular remodeling in apoE-null mice occurs in a strain-dependent manner: B6-apoE mice enlarge the diameter of the aortic arch, whereas 129-apoE mice widen the curvature of the aortic arch.

Plaque areas at the aortic arch and root

The plaque areas at the aortic arch measured using the captured images (Figure 1F) were in concordance with the cross-sectional plaque sizes in the apoE-null mice (R^2=0.83, p<0.0001, n=48, Supplemental Figure 2A and 2B). The plaque areas in the inner curvature of the aortic arch measured using captured images were significantly greater in 129-apoE than in B6-apoE mice at 3 months (25.9±1.7 vs 4.7±1.3 $\times 10^4 \mu m^2$, p<0.001) and at 9 months (294.8±24.8 vs 126.1±13.7 $\times 10^4 \mu m^2$, p<0.0001)(Figure 1G). In contrast, the plaque areas at the aortic root of the same animals at 3 months were significantly smaller in 129-apoE than in B6-apoE mice (0.7±0.1 vs 2.8±0.9 $\times 10^4 \mu m^2$, p<0.05), but those at 9 months were similar (44.8±7.9 vs 36.0±2.0 $\times 10^4 \mu m^2$, p=0.51)(Supplemental Figure 2C and 2D).

Mean velocities at the ascending and descending aorta

To evaluate hemodynamic parameters, we measured time-average mean velocities at the ascending and the descending aorta (mVAA and mVDA) using Doppler ultrasound (Figure 2A and 2B). mVAA was significantly lower in 129-apoE mice at 9 months than in B6-apoE mice (601±15 vs 738±42 mm/s, p<0.01, Figure 2C), although no strain effect on mVAA was found by three-way ANOVA (Supplemental Table). In contrast, mVDA was significantly lower in the 129 strain than in the B6 strain (p<0.0001), particularly in apoE-null mice at 9 months (437±33 vs 640±35 mm/s, p<0.01, Figure 2D). Of note, mVAA was significantly higher in B6-apoE mice at 9 months than in B6-WT mice at 9 months (738±42 vs 595±35 mm/s, p<0.05). Furthermore, mVDA was significantly lower in 129-apoE mice at 9 months than in 129-WT mice at 9 months (437±33 vs 554±17 mm/s, p<0.05). Thus, the hemodynamics of apoE-null mice at 9 months differ from the corresponding WT-mice in a strain-dependent manner.

Relative WSS

The time-averaged WSS in the ascending and descending aorta is approximately proportional to the systolic-average maximum velocity divided by the aortic diameter, mVAA/AA and mVDA/DA respectively. We will refer to these ratios as “relative” wall shear stress (rWSS), in the sense that they can be used in a relative sense to compare the WSS in different strains, genotypes and regions. The ratio mVAA/AA was larger in the 129 strain and there were significant age, strain, and genotype effects on mVAA/AA by three-way ANOVA (p<0.05, p<0.001, and p<0.05, respectively, Supplemental Table), although the difference between the 129-apoE and B6-apoE mice at 9 months was not significant (523±33 vs 474±26 s^{-1}, p=0.27, Figure 3A). In contrast, mVDA/DA was smaller in the 129 strain than in the B6 strain (p<0.01), particularly in apoE-null mice at 9 months (400±33 vs 533±32 s^{-1}, p<0.05, Figure 3B). The values of mVAA/AA in 129-WT and in 129-apoE mice at 3 months were significantly higher than mVDA/DA in each group (p<0.05 and p<0.001, respectively). However, mVAA/AA in B6-WT mice at 3 months was significantly lower than mVDA/DA (p<0.05), but these ratios were not different in B6-apoE mice at 3 months.

The mVAA/AA values in apoE-null mice at 9 months were negatively correlated with arch plaque size after adjusting for strain (R^2=0.83, p<0.01), significantly in B6-apoE mice (R^2=0.64, p<0.01), but less so in 129-apoE mice (R^2=0.40, p=0.07)(Supplemental Figure 3A). Similarly, mVDA/DA in 9-month-old apoE-null mice was negatively correlated with arch plaque size after adjusting for strain (R^2=0.82, p<0.01), significantly in 129-apoE mice (R^2=0.60, p<0.05), and less so in B6-apoE (R^2=0.32, p=0.12)(Supplemental Figure 3B).

To estimate the mean rWSS over the entire aortic arch, we averaged the mVAA/AA and mVDA/DA values in each mouse. There was a significant genotype effect on the mean rWSS by three-way ANOVA ($p<0.05$), but not strain and age effects (Supplemental Table). Also there was a significant interaction between age and genotype ($p<0.01$), reflecting the reduction of mean rWSS with age seen only in the apoE-null strains (significantly in the 129-apoE mice, Figure 3C). The arch plaque sizes at 9 months were negatively correlated with the mean rWSS for both the 129-apoE and B6-apoE mice ($R^2=0.60$, $p=0.01$ for each, and $R^2=0.86$, $p<0.0001$ after adjusting for strain, Figure 3D). Importantly, the two regression lines were almost parallel (no interaction between strain and mean rWSS, $p=0.43$), suggesting that the contribution of WSS to arch plaque size is independent of strain. No correlations between the mean rWSS in the aortic arch and root lesions were observed.

Local flow asymmetry in the two strains

The local flow asymmetry across the aortic lumen at stations in the ascending and descending aorta was assessed using another set of 9-month-old WT and apoE-null mice (Figure 4). We found an asymmetrical flow pattern at the ascending aorta, where systolic mean velocity along the outer curvature was higher than the velocity along the inner curvature in both WT and apoE-null mice. This asymmetry, however, was diminished in the descending aorta, especially in apoE-null mice. No strain differences in the asymmetrical flow pattern were observed (Figure 4C and 4D). Additionally, there were no significant strain differences in early diastolic TVI in both WT and apoE-null mice (Figure 4E and 4F). Furthermore, no correlations between arch plaques and early diastolic TVI were found at the ascending aorta ($R^2=0.14$, $p=0.21$, $n=9$) or the descending aorta ($R^2=0.05$, $p=0.39$, $n=9$) in apoE-null mice after adjusting for strain.

Discussion

In agreement with earlier work (11), we find that anatomical parameters of the aortic arch and mean flow velocities at the ascending and descending aorta are different for the 129 and B6 strains of WT mice. Furthermore, as plaques develop in the aortic arch of apoE-null mice, these differences become exaggerated in a strain-dependent manner. Significant negative correlations between mean rWSS and arch plaques in the two strains of apoE-null mice indicate a strain-independent role of WSS in arch plaque development.

The B6 strain had a larger aortic diameter at the AA than the 129 strain and a reduced aortic diameter at the DA compared to the AA diameter. In contrast, the 129 strain had more consistent aortic diameters. This differential geometric feature between the two strains might be to some extent responsible for the lower flow velocity at the DA in the 129 strain, as the reduced DA diameter (relative to the AA diameter) in the B6 strain might cause higher velocity. In addition, although both strains of WT and apoE-null at 9 months show similar levels of systemic blood pressure, both cardiac output and heart rate were significantly higher in the B6 strain than in the 129 strain. Differences in cardiac function undoubtedly contribute to the strain differences in systolic flow velocity observed in apoE-null mice.

Another possible explanation for strain-specific differences of hemodynamics at the ascending and descending aorta is arterial remodeling. For example, atherosclerotic human coronary arteries have been shown to enlarge, preserving luminal area to maintain blood flow (15). However, as atherosclerotic plaques grow in size, the lumen area narrows and results in a reduced blood flow. This phenomenon has been also observed in atherosclerotic mouse models (16,17). In addition, the vascular wall response to left carotid artery ligation is greater in FVB/NJ and SJL/J strains than in the C3H/HeJ strain, indicating that vascular remodeling in mice is genetically controlled (18,19). Indeed, we showed a strain-dependent

vascular remodeling in apoE-null mice at 9 months of age: the aortic arch of the B6 strain had an exaggerated enlargement of diameter, whereas the 129 strain exhibited an exaggerated flattening of the top of the arch. Such changes in vascular geometry, in addition to the presence of intrusive plaques, can have an important effect on arch hemodynamics.

The flow pattern in the aortic arch is asymmetrical, with the highest velocity along the outer curvature and with the lowest velocity along the inner curvature (20,21,22). Similarly, we found an asymmetrical flow pattern across the aortic lumen at the ascending aorta, and to some extent at the descending aorta. However, no strain differences in the asymmetrical flow pattern at either location were observed. Additionally, both experimental and clinical data show that the oscillatory flow pattern associated with aortic regurgitation (AR) increases atherosclerosis in the descending aorta (20,23,24). Interestingly, the AR severity, measured by early diastolic TVI, correlated positively with plaques in the descending aorta, while it was negatively correlated with the presence of plaques in the aortic arch in low-density lipoprotein receptor-null mice (20). In the present study, we found no strain differences in early diastolic TVI in either WT-mice or apoE-null mice, and no correlation between arch plaques and early diastolic TVI. These findings suggest that oscillatory flow along the inner curvature is less likely to be a major cause of the strain difference in plaque development of the aortic arch.

It is commonly accepted that atherosclerotic lesions develop more in the area exposed to lower WSS (25). Our previous computer simulation showed lower levels of WSS at the inner curvature of the arch in 129-WT mice than in B6-WT mice (11), consistent with greater plaque areas at the aortic arch in the 129-apoE mice. In the present study, the relative shear in the descending aorta (mVDA/DA) was similarly lower in the 129 strain, particularly in apoE-null mice at 9 months, though no strain effect was seen in the ascending aorta. One limitation of our study is that we measured mean flow velocity and vessel diameter only at two points, one each in the ascending and descending aorta. A simple estimate of shear was used to compare mouse strain and genotype. In reality, atherosclerosis is a disease that begins locally and is mediated by local hemodynamics that are not captured by our global estimates of shear. Our results do suggest, however, that the effect of overall differences in geometry and flow, due to strain or genotype, can be reflected in the overall level of disease. Indeed, in spite of these limitations and strain differences in vascular geometry and hemodynamics, the arch plaque sizes were negatively correlated with the mean rWSS within each strain of 9-month-old apoE-null mice. Interestingly, the two regression lines were nearly parallel, suggesting a strain-independent role of WSS in arch plaque development.

Blood viscosity, which is mainly determined by hematocrit levels, affects WSS *in vivo* and is a predictor of coronary heart disease in humans (25-27). Joven's group reported that hematocrit levels were positively correlated with blood viscosity and with plaque size at the aortic root in apoE-null mice on a mixed genetic background of B6 and 129/Ola strains (28,29). In the present study, we showed that hematocrit levels in both WT and apoE-null mice were significantly higher in the 129 strain than in the B6 strain, although there were no significant relationships between hematocrit levels and plaque sizes at either the aortic arch or root in the individual animal ($p=0.33$ and $p=0.84$, respectively, after adjusting for strain). The higher hematocrit levels in 129-apoE mice may indirectly contribute to plaque development through alterations in hemostatic and hemorheological processes (26).

We have recently identified several quantitative trait loci (QTLs) in a cross between 129-apoE and B6-apoE mice that affect plaque development at the aortic arch and root, and aspects of the geometry of the aortic arch (10). Remarkably, the QTLs for susceptibility to atherosclerosis in the arch overlapped with the QTL that affects curvature of the arch, suggesting that developmental genetic factors governing the shape of the vessel could be

risk factors for atherosclerosis. We also identified an overlapping QTL for arch plaque size and total cholesterol levels, suggesting genetic interactions between atherosclerosis and plasma lipid levels in this cross. Indeed, plasma lipid levels are higher in 129-apoE mice than in B6-apoE mice, and total cholesterol levels were significantly correlated with arch lesion size in 9-month-old apoE-null mice (R^2=0.84, p=0.001 after adjusting for strain). Additionally, two 129 substrains (129P3/J and 129X1/SvJ) have been reported to exhibit impaired endothelium-dependent relaxation of the aorta in response to acetylcholine compared to C57BL/6J strain (30). Consequently, aortic vessels of the 129 strains could respond differentially to a similar level of WSS, and together with increased blood viscosity and cholesterol concentration contribute to increased atherosclerosis susceptibility.

In conclusion, our study using an inbred mouse model pair, 129-apoE and B6-apoE mice, showed that vascular geometry, hemodynamics, and the changes in geometry that accompany plaque formation are strain-dependent. However, when these strain-dependent physiological data were integrated into the parameter corresponding to mean rWSS, a strain-independent negative relationship with arch plaque size emerged. These findings imply an important role for WSS in arch plaque development in mice of either strain. Flow in the aortic arch is not simple, which includes disturbed flow and oscillatory flow. Changes in vascular geometry with age and by plaques also complicate the relationships between WSS and plaque development in this location. Longitudinal study of hemodynamics and atherosclerosis in individual mice would clarify the extent to which WSS variations are responsible for inter-strain differences in aortic arch atherosusceptibility.

Supplementary Material

Refer to Web version on PubMed Central for supplementary material.

Acknowledgments

We gratefully thank Oliver Smithies for discussion, Tomohiro Osanai for critical reading of the manuscript, and Svetlana Zhilicheva, Shinja Kim, Hyung-Suk Kim, and Feng Li for their excellent technical support.

Funding This work was supported by a NIH grant HL42630 to N. Maeda and an American Heart Association Fellowship Award 09POST2250823 to H. Tomita.

References

1. Friedman MH, Deters OJ, Mark FF, Bargeron CB, Hutchins GM. Arterial geometry affects hemodynamics. A potential risk factor for atherosclerosis. Atherosclerosis. 1983; 46:225–31. [PubMed: 6838702]
2. Nerem RM. Atherogenesis: Hemodynamics, vascular geometry, and the endothelium. Biorheology. 1984; 21:565–9. [PubMed: 6487767]
3. Chatzizisis YS, Coskun AU, Jonas M, Edelman ER, Feldman CL, Stone PH. Role of endothelial shear stress in the natural history of coronary atherosclerosis and vascular remodeling: Molecular, cellular, and vascular behavior. J Am Coll Cardiol. 2007; 49:2379–93. [PubMed: 17599600]
4. Friedman MH, Baker PB, Ding Z, Kuban BD. Relationship between the geometry and quantitative morphology of the left anterior descending coronary artery. Atherosclerosis. 1996; 125:183–92. [PubMed: 8842350]
5. Ding Z, Biggs T, Seed WA, Friedman MH. Influence of the geometry of the left main coronary artery bifurcation on the distribution of sudanophilia in the daughter vessels. Arterioscler Thromb Vasc Biol. 1997; 17:1356–60. [PubMed: 9261267]
6. Schulz UG, Rothwell PM. Major variation in carotid bifurcation anatomy: A possible risk factor for plaque development? Stroke. 2001; 32:2522–9. [PubMed: 11692011]

7. Thomas JB, Antiga L, Che SL, Milner JS, Steinman DA, Spence JD, Rutt BK. Variation in the carotid bifurcation geometry of young versus older adults: Implications for geometric risk of atherosclerosis. Stroke. 2005; 36:2450–6. [PubMed: 16224089]
8. Zhang SH, Reddick RL, Piedrahita JA, Maeda N. Spontaneous hypercholesterolemia and arterial lesions in mice lacking apolipoprotein E. Science. 1992; 258:468–71. [PubMed: 1411543]
9. Maeda N, Johnson L, Kim S, Hagaman J, Friedman M, Reddick R. Anatomical differences and atherosclerosis in apolipoprotein E-deficient mice with 129/SvEv and C57BL/6 genetic backgrounds. Atherosclerosis. 2007; 195:75–82. [PubMed: 17275002]
10. Tomita H, Zhilicheva S, Kim S, Maeda N. Aortic arch curvature and atherosclerosis have overlapping quantitative trait loci in a cross between 129S6/SvEvTac and C57BL/6J apolipoprotein E-null mice. Circ Res. 2010; 106:1052–60. [PubMed: 20133902]
11. Zhu H, Zhang J, Shih J, Lopez-Bertoni F, Hagaman JR, Maeda N, Friedman MH. Differences in aortic arch geometry, hemodynamics, and plaque patterns between C57BL/6 and 129/SvEv mice. J Biomechanical Eng. 2009; 131:121005.
12. Hartley CJ, Reddy AK, Madala S, Martin-McNulty B, Vergona R, Sullivan ME, Halks-Miller M, Taffet GE, Michael LH, Entman ML, Wang YX. Hemodynamic changes in apolipoprotein E-knockout mice. Am J Physiol Heart Circ Physiol. 2000; 279:H2326–34. [PubMed: 11045969]
13. Zhou YQ, Foster FS, Nieman BJ, Davidson L, Chen XJ, Henkelman RM. Comprehensive transthoracic cardiac imaging in mice using ultrasound biomicroscopy with anatomical confirmation by magnetic resonance imaging. Physiol Genomics. 2004; 18:232–44. [PubMed: 15114000]
14. Feintuch A, Ruengsakulrach P, Lin A, Zhang J, Zhou YQ, Bishop J, Davidson L, Courtman D, Foster FS, Steinman DA, Henkelman RM, Ethier CR. Hemodynamics in the mouse aortic arch as assessed by MRI, ultrasound, and numerical modeling. Am J Physiol Heart Circ Physiol. 2007; 292:H884–92. [PubMed: 17012350]
15. Glagov S, Weisenberg E, Zarins CK, Stankunavicius R, Kolettis GJ. Compensatory enlargement of human atherosclerotic coronary arteries. N Engl J Med. 1987; 316:1371–5. [PubMed: 3574413]
16. Bonthu S, Heistad DD, Chappell DA, Lamping KG, Faraci FM. Atherosclerosis, vascular remodeling, and impairment of endothelium-dependent relaxation in genetically altered hyperlipidemic mice. Arterioscler Thromb Vasc Biol. 1997; 17:2333–40. [PubMed: 9409199]
17. Seo HS, Lombardi DM, Polinsky P, Powell-Braxton L, Bunting S, Schwartz SM, Rosenfeld ME. Peripheral vascular stenosis in apolipoprotein E-deficient mice. Potential roles of lipid deposition, medial atrophy, and adventitial inflammation. Arterioscler Thromb Vasc Biol. 1997; 17:3593–601. [PubMed: 9437210]
18. Harmon KJ, Couper LL, Lindner V. Strain-dependent vascular remodeling phenotypes in inbred mice. Am J Pathol. 2000; 156:1741–8. [PubMed: 10793085]
19. Korshunov VA, Berk BC. Strain-dependent vascular remodeling: The “Glagov phenomenon” is genetically determined. Circulation. 2004; 110:220–6. [PubMed: 15226209]
20. Zhou YQ, Zhu SN, Foster FS, Cybulsky MI, Henkelman RM. Aortic regurgitation dramatically alters the distribution of atherosclerotic lesions and enhances atherogenesis in mice. Arterioscler Thromb Vasc Biol. 2010; 30:1181–8. [PubMed: 20299687]
21. Bogren HG, Mohiaddin RH, Kilner PJ, Jimenez-Borreguero LJ, Yang GZ, Firmin DN. Blood flow patterns in the thoracic aorta studied with three-directional MR velocity mapping: the effects of age and coronary artery disease. J Magn Reson Imaging. 1997; 7:784–93. [PubMed: 9307902]
22. Janiczek RL, Blackman BR, Roy RJ, Meyer CH, Acton ST, Epstein FH. Three-dimensional phase contrast angiography of the mouse aortic arch using spiral MRI. Magn Reson Med. 2011 in press, doi: 10.1002/mrm.22937.
23. Shimoni S, Zilberman L, Edri O, Bar I, Goland S, Gendelman G, Swissa M, Livshitz S, Paz O, Ayzenberg O, George J. Thoracic aortic atherosclerosis in patients with aortic regurgitation. Atherosclerosis. 2011; 218:107–9. [PubMed: 21696740]
24. Cheng C, Tempel D, van Haperen R, van der Baan A, Grosveld F, Daemen MJ, Krams R, de Crom R. Atherosclerotic lesion size and vulnerability are determined by patterns of fluid shear stress. Circulation. 2006; 113:2744–53. [PubMed: 16754802]

25. Malek AM, Alper SL, Izumo S. Hemodynamic shear stress and its role in atherosclerosis. JAMA. 1999; 282:2035–42. [PubMed: 10591386]

26. Koenig W, Ernst E. The possible role of hemorheology in atherothrombogenesis. Atherosclerosis. 1992; 94:93–107. [PubMed: 1632876]

27. de Simone G, Devereux RB, Chien S, Alderman MH, Atlas SA, Laragh JH. Relation of blood viscosity to demographic and physiologic variables and to cardiovascular risk factors in apparently normal adults. Circulation. 1990; 81:107–17. [PubMed: 2297818]

28. Paul A, Calleja L, Vilella E, Martinez R, Osada J, Joven J. Reduced progression of atherosclerosis in apolipoprotein E-deficient mice with phenylhydrazine-induced anemia. Atherosclerosis. 1999; 147:61–8. [PubMed: 10525126]

29. Tous M, Ferre N, Vilella E, Riu F, Camps J, Joven J. Circulating blood cells modulate the atherosclerotic process in apolipoprotein E-deficient mice. Metabolism. 2004; 53:95–100. [PubMed: 14681849]

30. Ryan MJ, Didion SP, Davis DR, Faraci FM, Sigmund CD. Endothelial dysfunction and blood pressure variability in selected inbred mouse strains. Arterioscler Thromb Vasc Biol. 2002; 22:42–8. [PubMed: 11788459]

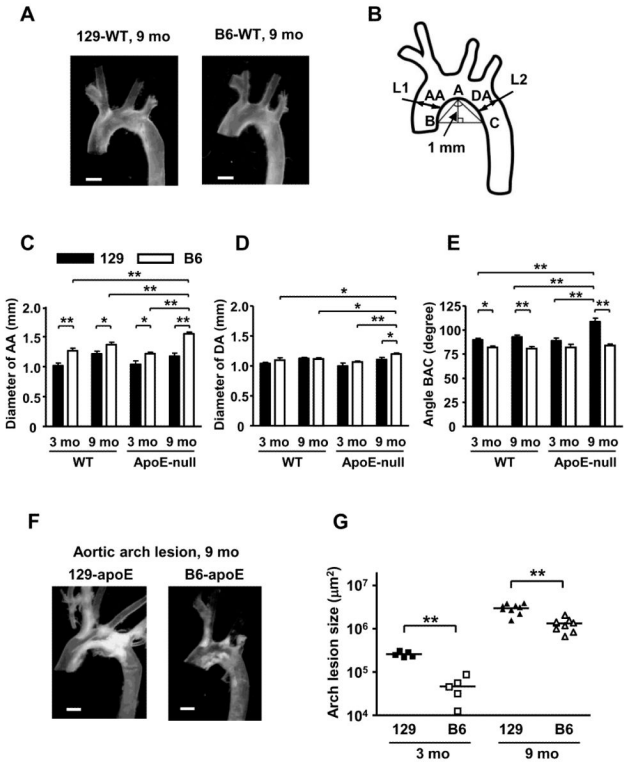

Figure 1.

A. Representative images of excised aortas from 9-month-old 129-WT and B6-WT mice (Scale bar, 1 mm). B. Schema representing angle of the aortic arch (angle BAC), diameters of the ascending aorta (AA) and descending aorta (DA), and locations where flow velocity was measured (L1 and L2). C. Diameter of AA in each group. D. Diameter of DA in each group. E. Angle BAC in each group. F. Representative images of excised aortas from 9-month-old 129-apoE and B6-apoE mice (Scale bar, 1 mm). G. Comparison of plaque lesion size at the aortic arch in each apoE-null mouse. *p<0.05 and **p<0.01.

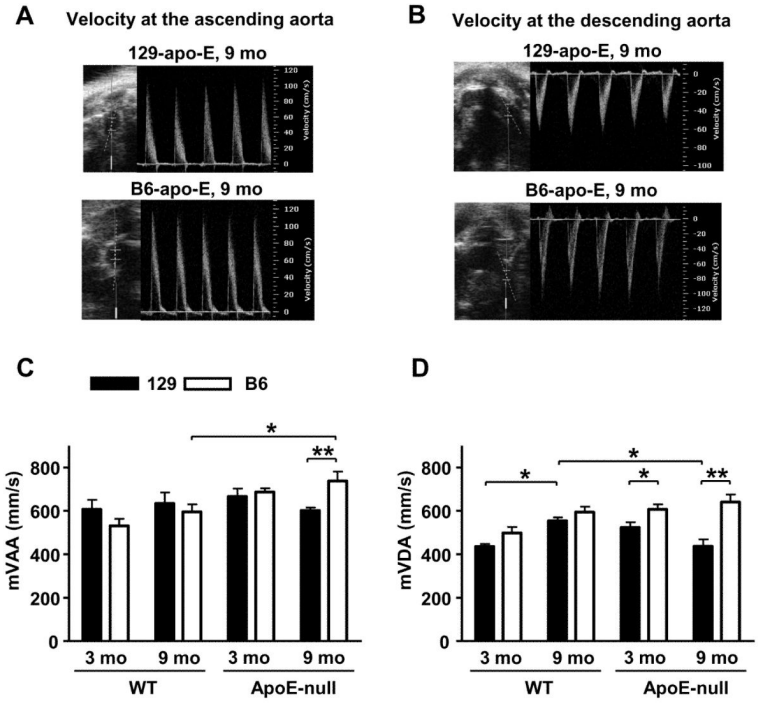

Figure 2.

A and B. Representative velocity signals at the ascending and descending aorta of 129-apoE and B6-apoE mice at 9 months. C and D. Mean flow velocities at the ascending and descending aorta (mVAA and mVDA) in each group. *p<0.05 and **p<0.01.

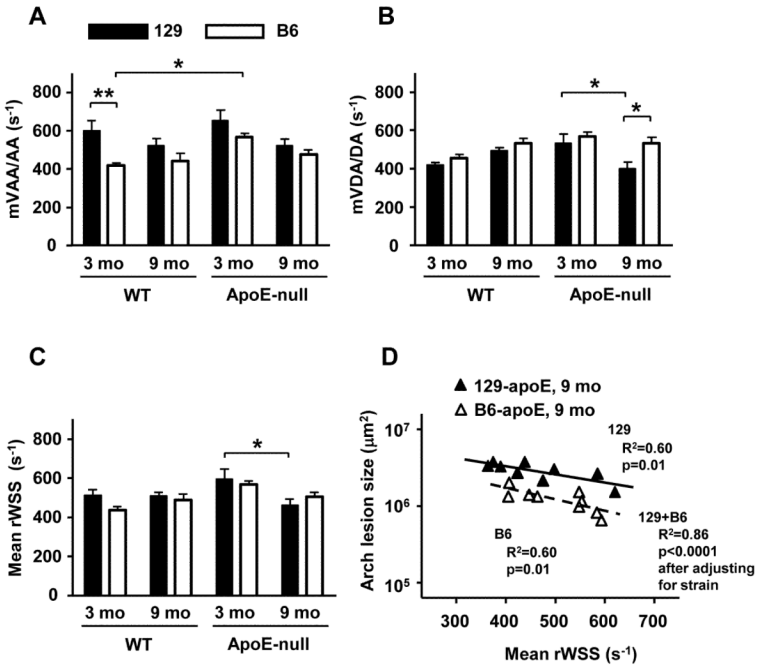

Figure 3.

A. Relative WSS (rWSS) at the ascending aorta (mVAA/AA) in each group. B. rWSS at the descending aorta (mVDA/DA) in each group. C. Mean rWSS over the entire aortic arch ((mVDA/DA + mVAA/AA)/2) in each group. D. Relationship between mean rWSS and arch plaque lesion sizes in 9-month-old 129-apoE and B6-apoE mice.

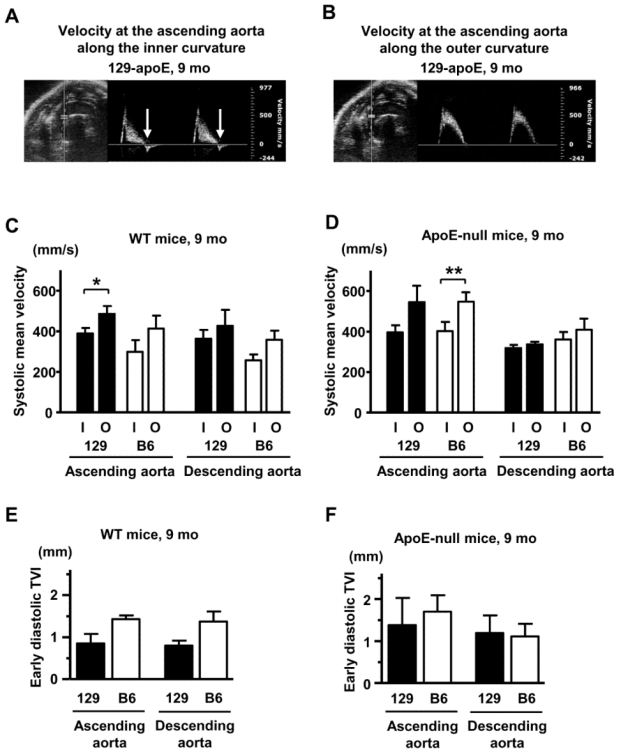

Figure 4.

A and B, Representative velocity signals at the ascending aorta along the inner curvature (A) and the outer curvature (B) in 129-apoE mice at 9 months. Arrows indicate early diastolic retrograde flow. C and D, Systolic mean flow velocity at the ascending and descending aorta along the inner curvature (I) and the outer curvature (O) in WT-mice (C) and in apoE-null mice (D) at 9 months. E and F, Early diastolic time-velocity integral (TVI) along the inner curvature at the ascending and descending aorta in WT-mice (E) and in apoE-null mice (F). *p<0.05 and **p<0.01. n=4-5.

Table 1

Profiles of WT and apoE-null mice we studied.

	WT 3 months		WT 9 months		ApoE-null 3 months		ApoE-null 9 months		Effects (p value)			
	129 (n=5)	B6 (n=5)	129 (n=7)	B6 (n=7)	129 (n=5)	B6 (n=5)	129 (n=9)	B6 (n=9)	Age	Strain	Genotype	Interactions
BW (g)	23.3±0.8	24.9±1.1	28.1±0.9	36.8±1.4*	21.8±1.1	27.1±0.3*	29.3±1.5	33.3±0.4*	<0.0001	<0.0001	ns	*a*
Cholesterol (mg/dL)	94±4	83±4	93±4	82±2*	879±73	496±17*	745±23	540±49*	ns	<0.0001	<0.0001	*b*
Triglyceride (mg/dL)	54±11	70±12	51±3	60±4	75±11	131±11*	166±24	144±24	ns	ns	<0.0001	*c*
HDL-C (mg/dL)	77±7	61±4	101±4	83±2*	96±12	101±8	137±19	75±10*	ns	<0.01	<0.01	*d*
Hematocrit (%)	40±1	37±1*	42±1	37±1*	46±2	37±1*	45±1	33±1*	ns	<0.0001	ns	*e*
Platelet (10^9/L)	431±32	765±26*	328±94	936±111*	564±50	896±45*	626±38	1354±92*	<0.05	<0.0001	<0.0001	*f*
Heart (mg)	150±12	136±6	195±4	205±10	161±14	162±4	189±9	200±8	<0.0001	ns	ns	ns
Heart/BW (mg/g)	6.4±0.3	5.5±0.2*	7.0±0.2	5.6±0.2*	7.4±0.7	6.0±0.1	6.5±0.3	6.0±0.2	ns	<0.0001	ns	ns
Fractional shortening (%)	29±2	34±4	30±1	28±2	30±2	33±2	28±2	36±1*	ns	<0.05	ns	ns
Stroke volume (μL)	25±4	35±3	35±3	33±5	34±2	28±4	35±2	41±3	<0.05	ns	ns	*a*
Heart rate (beats/min)	422±11	533±18*	426±12	491±19*	413±11	532±11*	404±10	500±12*	ns	<0.0001	ns	ns
Cardiac output (mL/min)	11±2	19±2*	15±1	16±3	14±1	15±2	14±1	21±2*	ns	<0.001	ns	*a*

Values are mean±SEM.

*p<0.05 vs 129 strain within each group. BW indicates body weight; ns, not significant;

a p<0.05 for AgexStrainxGenotype;

b p<0.0001 for StrainxGenotype;

c p<0.05 for AgexGenotype;

d p<0.05 for AgexStrain and p<0.05 for AgexStrainxGenotype;

e p<0.01 for StrainxGenotype;

f p<0.01 for AgexStrain.